World Applied Sciences Journal 6 (1): 129-143, 2009
ISSN 1818-4952

Performance of Elbow-bend Heat Exchangers Having Air Side and Water Tube Bank with Different Arrangements

A.A. El-Ehwany, G.M. Hennes, E.I. Eid and E. El-Kenany

Mechanical Power Department, Faculty of Engineering, Ain Shams University, Egypt

Abstract: In this work the effect of the elbow-bend geometry and the effect of the tube arrangement on the performance of air-to-water heat exchanger are studied experimentally. In elbow-bend the exit direction of the air; which is the working fluid outside the tubes is bended at 90 degrees to its inlet direction. Three different types of the geometry of the elbow with three different tube bank arrangements are suggested to study. The results were plotted and analyzed to clarify the effects of the elbow bend geometry and the tube bank arrangements as well as the dead volume on the heat exchange and friction factor *f*. Two empirical relations were correlated for each design, one to predict the relation between *Nusselt* number and *Reynolds* number, while the other relation is between the friction factor *f* and *Reynolds* number. This was done to select the best design to be used in a Stirling engine design.

Key words: Stirling engines · Heat exchangers

INTRODUCTION

Stirling engines can be operated by various heat sources. Referring to the literature of Stirling engines, different designs of the heat exchangers are found. Some of which are explained below.

A small gamma-type Stirling engine was tested by Iwamoto *et al*. [1]. In this engine the heat exchangers are located around the displacer cylinder. The heater and the cooler are of the fine-tube type. Hot water flows in the heater tubes. Cooling water flows in the cooler tubes. The working gas flows around these tubes.

Hoshino [2] used twelve electrical heaters attached to a gamma-type Stirling engine heater head. The working gas is heated through annular flow passages of the groove-type heater, each of which has 25 plate fins around the cylindrical heater. The cooler is of a shell and tube type, which has 322 tubes of 1 mm inner diameter.

A heat input system which is composed of a heater and a burner as a newly devised heat exchanger in a Beta type Stirling engine was designed and tested by Chang [3]. The heater is shaped like a U-cup and has slits which play the role of the heater tubes on the outer wall of the cup.

A 200 W domestic free-piston Stirling electric power system with multi-fuel capability was designed by Biao and Xianrui [4]. The engine is fitted with a fine heater and an annular shaped clearance regenerator. The cylinder head is provided with vertical fins. At operation, the hot gases flow along the vertical fins and the heat is supplied to the helium working gas through these fins.

A thermodynamic analysis of a Stirling engine including dead volumes of hot space, cold space and regenerator was carried out by Kongtragool *et al.* [5]. The analysis indicated that the engine net work is affected by only the dead volumes while the efficiency is affected by both the regenerator effectiveness and dead volumes.

The heat transfer characteristics and pressure drop of block-type heat exchangers were experimentally investigated by El-Ehawany *et al.* [6]. The experimental data were compared to get the most suitable block-type heat exchanger to be used as a cooler and a heater in Stirling machines.

Generalized correlations of heat transfer and friction factor for air side plain fin-and-tube heat exchangers were reported by Wang *et al.* [7], where 31 samples of fin-and-tube heat exchangers were used to develop the correlations.

An experimental study to investigate the heat transfer and friction characteristics of fin-and-tube heat exchangers was carried out by Yan and Sheen [8]. The results were presented as plots of friction factor *f* and Colburn *j* factor versus Reynolds number.

Corresponding Author:A.A. El-Ehwany, Mechanical Power Department, Faculty of Engineering, Ain Shams University, Egypt

Kim *et al.* [9] used a multiple regression technique to correlate the data of 47 sets of plain fin-and-tube heat exchangers with staggered tube arrangements to develop the heat transfer and friction correlations.

The design of a heat exchanger requires a balanced approach between the thermal design and pressure drop. The pressure drop results in the increase of the operating cost of fluid moving devices such as pumps and fans. This shows that the design of heat exchangers should not concern only with the capacity of heat transfer, but also with the pressure drop across the heat exchanger. The tube bank arrangements are common configurations in heat exchangers.

Figure 1 shows a schematic diagram of the main parts of the alpha type Stirling engine. It is clear that both of the heater and the cooler are located at the two corners of the engine. The path of the working fluid is bent at right angle inside the heater and the cooler.

In the present work, an elbow-bend shell-and-tube heat exchanger was introduced as a new design for the heater and cooler of alpha-type Stirling engine. The elbow-bend heat exchanger is formed of a shell in the form of a right-angle elbow and a tube bank fitted perpendicular to the flow across the elbow. Eight specimens of these heat exchangers were designed, manufactured and tested during the experimental study of this work. The experimental investigation is pointed at the influence of the elbow bend geometry, tube bank arrangement and dead volume on the thermal performance and pressure drop of the elbow bend heat exchanger. The dead volume is the difference between the elbow volume and the volume occupied by the tubes.

EXPERIMENTAL APPARATUS

Figure 2 shows a schematic diagram of the test rig used in this work. It consists of a wind tunnel system to suck hot air past the outside surface of the tube bank by a 3 *HP* centrifugal fan. Water at room temperature was pumped through the tube bank which was designed to circulate the cold water through five or six passes. The air duct was a circular duct of 52.3 mm or 104.6 mm inner diameter. The air flow rate was measured by using one of two orifice plates (one for each duct) that were designed and manufactured according to BSI data catalog, [10]. The air flow rate was controlled by a regulating gate valve. The air was heated by five heaters having a total power of 10.75 *kW* in the heating box. Four heaters were connected directly to the main supply, while the last one was connected through a voltage regulator. The air temperature was adjusted at 146±1.5°C at the inlet of the test section. The water was supplied through a tank with a float supported at 7m above the test section to sustain a constant water flow rate during the experiments. The water flow rate was measured by a tank having a definite volume and a stop watch. The temperature was measured by thirty one pre-calibrated *T*-type thermocouples. The inlet and exit temperatures of air were measured by two thermocouple meshes. Each mesh consists of 13 thermocouples connected in parallel to evaluate the average temperature [11]. The inlet and exit temperatures of the cooling water were measured by two thermocouples; one at inlet and the other at the water exit. The tube surface temperature was measured by using two thermocouples. The air temperature at the orifice plate was measured by one thermocouple. The thermocouples were connected to a digital thermometer model 922 of 0.1°C resolution.

TEST SPECIMENS

Eight specimens were prepared of copper tubes of 0.25" (6.35 mm) outer diameter, 0.4 mm wall thickness and 120 mm long (tube total length). The tubes were soldered at 5 mm far from their ends to a pair of copper plates (headers) of 5 mm thick and 100 mm by 100 mm cross section as shown in Fig. 3. This means that the effective length of tube is 100 mm which is the distance between the two headers. Figure 4 shows a cross-section of the test specimen inside the shell. The header is square, quadrant, or combination of them. Eight heat exchangers of various elbow-bend geometries and tube bank arrangements were designed and manufactured. A schematic diagram of the tube bank arrangements and their center distances are shown in Fig. 5.

The complete geometrical data of the tube bank arrangements are demonstrated in Fig. 6 and 7, which show the headers of the heat exchangers with the holes for inserting the tubes. These headers clarify the geometry of the tube bank arrangement in each of the eight specimens.

EXPERIMENTAL PROCEDURE

1. The centrifugal fan was run.
2. The air mass flow rate was adjusted at the required value.
3. The electrical heaters were switched on at the required value.

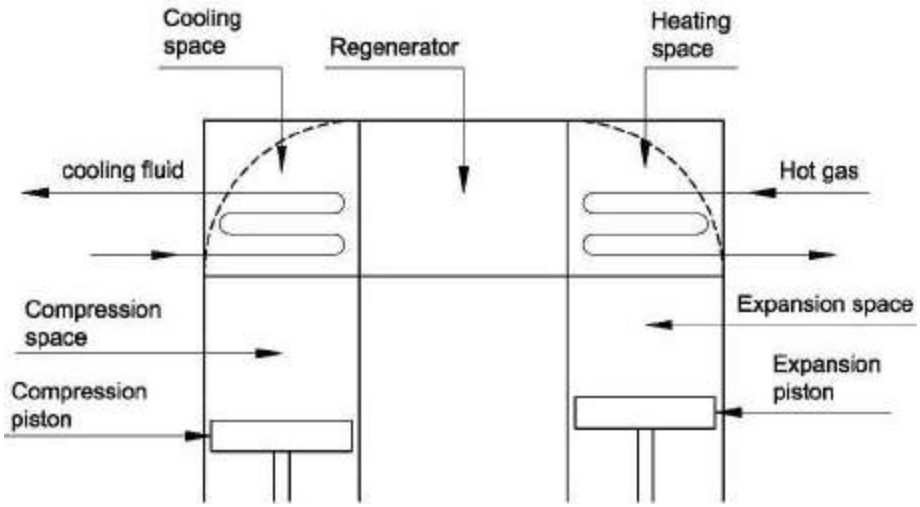

Fig. 1: Schematic diagram of the main parts of alpha type Stirling engine

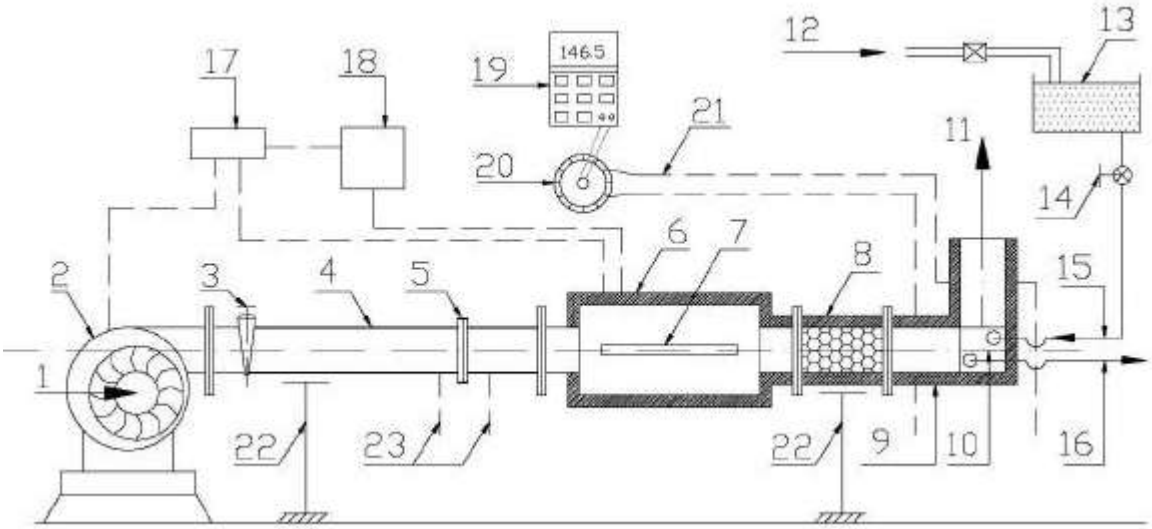

1- Air inlet
2- Air blower
3- Air regulating valve
4- Air duct
5- Orifice plate
6- Heating box
7- Electric Heaters
8- Mixing section
9- Test section
10- Test specimen
11- Air outlet
12- Water supply
13- Water tank
14- Water regulating valve
15- Water inlet
16- Water outlet
17- Electric power supply
18- Voltage regulator
19- Temperature measurement unit.
20- Rotary selector switch
21- Electric wires
22- Stand
23- To U-tube manometer

Fig. 2: Experimental test rig

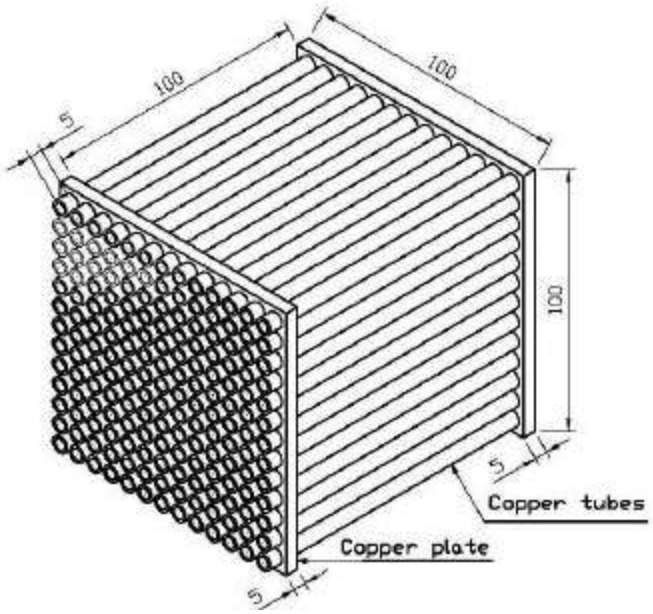

Fig. 3: Isometric of the test specimen No. II

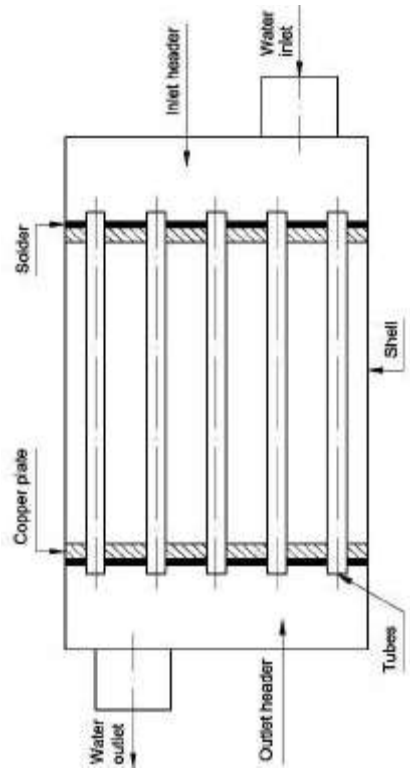

Fig. 4: Cross section of the test specimen inside the shell

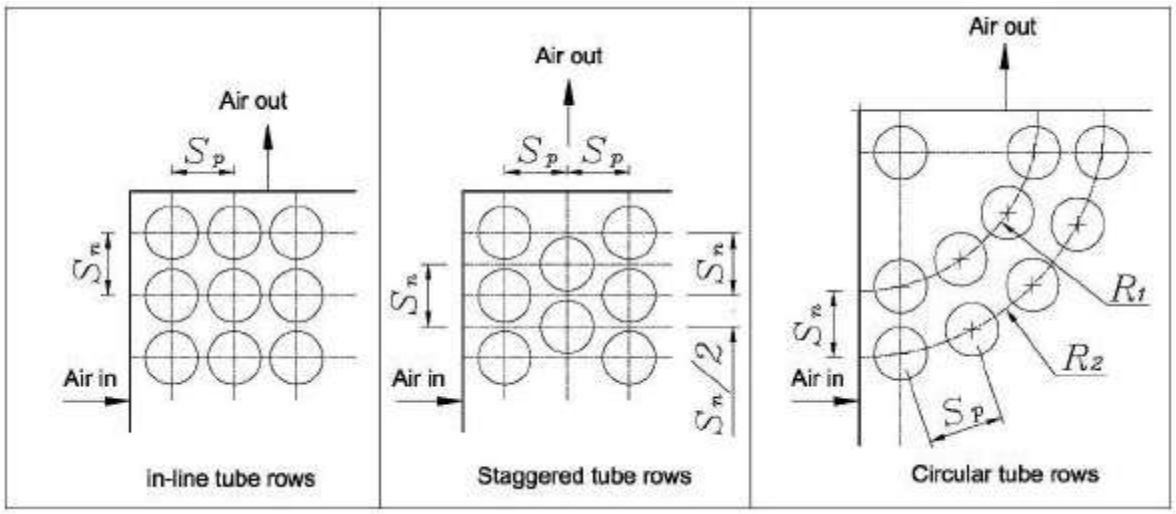

Fig. 5: Schematic diagram of the tube arrangements and its center distances

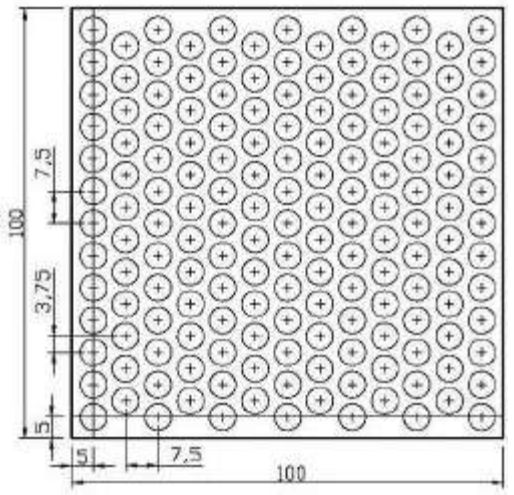

Specimen No. (I), 163 tubes (staggered arrangement), ψ =48.4 %, S_v = 325.17 m^{-1}
S_n=S_p=7.5 mm

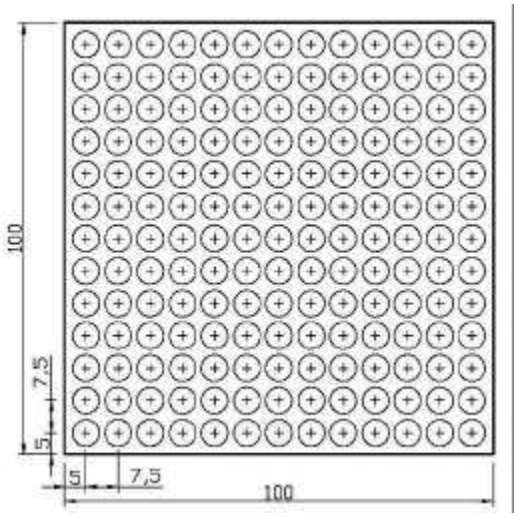

Specimen No. (II), 169 tubes (in-line arrangement), ψ =46.5 %, S_v = 337.14 m^{-1}
S_n=S_p=7.5 mm

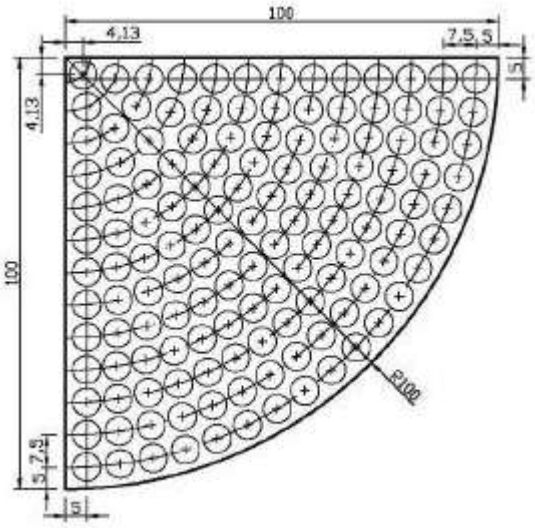

Specimen No. (III), 136 tubes (circular arrangement), ψ =45.2 % , S_v = 345.44 m^{-1}
19 tubes in the outer row,
S_n=7.5 mm, S_p=7.62 mm

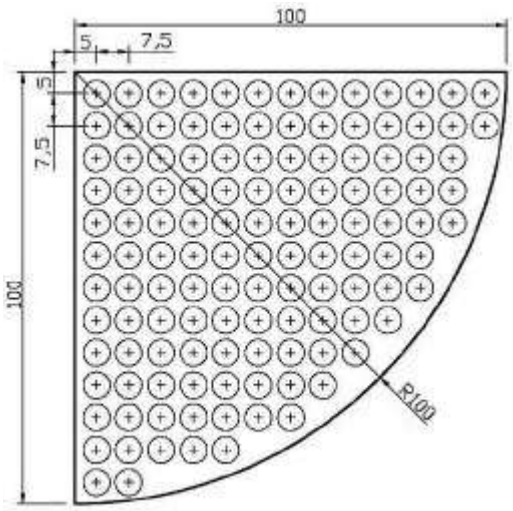

Specimen No. (IV), 125 tubes (in-line arrangement), ψ =49.6 % , S_v = 317.5 m^{-1}
S_n=S_p=7.5 mm

Fig. 6: Geometrical specifications of the test specimens No. I, II, III & IV

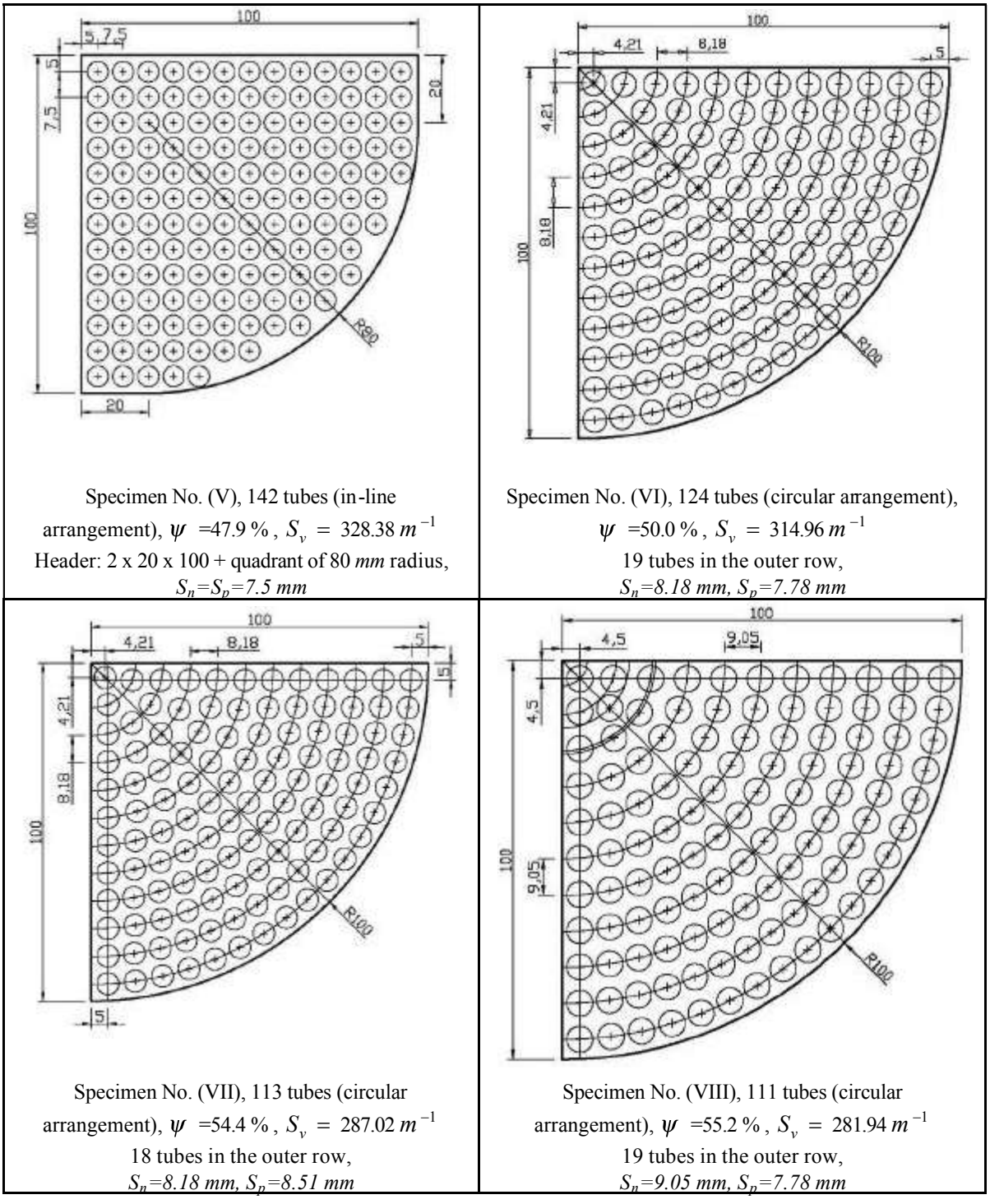

Specimen No. (V), 142 tubes (in-line arrangement), ψ =47.9 %, S_v = 328.38 m^{-1}
Header: 2 x 20 x 100 + quadrant of 80 *mm* radius,
S_n=S_p=*7.5 mm*

Specimen No. (VI), 124 tubes (circular arrangement), ψ =50.0 %, S_v = 314.96 m^{-1}
19 tubes in the outer row,
S_n=*8.18 mm*, S_p=*7.78 mm*

Specimen No. (VII), 113 tubes (circular arrangement), ψ =54.4 %, S_v = 287.02 m^{-1}
18 tubes in the outer row,
S_n=*8.18 mm*, S_p=*8.51 mm*

Specimen No. (VIII), 111 tubes (circular arrangement), ψ =55.2 %, S_v = 281.94 m^{-1}
19 tubes in the outer row,
S_n=*9.05 mm*, S_p=*7.78 mm*

Fig. 7: Geometrical specifications of the test specimens No. V, VI, VII &VIII

4. The cooling water valve was opened at the required water mass flow rate.
5. The values of the air mass flow rate, the temperature of the air at the inlet and the water mass flow rate had to be checked and readjusted if one of them was changed.
6. When the test system including the air and water sides became steady, the data signals were recorded.

DATA CALCULATIONS

The analysis of the present work is concerned with the calculation of nondimensional numbers for each experiment and deducing generalized correlations to explain the case study extensively. The following relations were used in the calculations. The properties of the air and the water were found at the film temperature [12].

$$h_a = \frac{\dot{Q}_a}{A_a\,(T_{a,ave} - T_{s,ave})} \quad (1)$$

$$h_w = \frac{\dot{Q}_w}{A_w\,(T_{s,ave} - T_{w,ave})} \quad (2)$$

$$Nu_a = \frac{h_a\,d_o}{k_a} \quad (3)$$

$$Nu_w = \frac{h_w\,d_i}{k_w} \quad (4)$$

$$G_{max} = \frac{\dot{m}_a}{A_{min}} \quad (5)$$

$$Re_a = \frac{\dot{m}_a\,d_o}{A_{min}\,\mu_a} \quad (6)$$

$$A_{min} = L\,(B - N_n\,d_o) \quad (7)$$

$$f = \frac{\Delta P_a\,\rho_{a,ave}}{2\,G_{max}^2\,N_p} \quad (8)$$

$$\varepsilon = \frac{\dot{Q}_{ave}}{\dot{Q}_{max}} = \frac{\dot{Q}_{ave}}{(\dot{m}C_p)_a\,(T_{i,a} - T_{i,w})} \quad (9)$$

$$NTU = \frac{U\,A}{C_{min}} \quad (10)$$

$$C^* = \frac{C_{min}}{C_{max}} = \frac{(\dot{m}\,c_p)_a}{(\dot{m}\,c_p)_w} \quad (11)$$

$$\frac{1}{U\,A} = \frac{1}{h_a\,A_a} + \frac{1}{h_w\,A_w} \quad (12)$$

neglecting the term $\frac{\ln(d_o/d_i)}{2\,\pi\,k_s\,L}$ which represents the thermal resistance of the tube wall thickness, which is too small.

$$\psi = \frac{V_d}{V_{total}} \quad (13)$$

$$S_v = \frac{A_a}{V_{total}} \quad (14)$$

RESULTS AND DISCUSSION

In Stirling engine, increasing both or one of the dead volume and the pressure drop of the heating and cooling spaces causes deteriorations of the engine power as well as the engine efficiency [7]. In the heat exchangers the pressure drop increases as the dead volume decreases. So, it is useful to make a comparison between the specimens according to the quantity ($\Delta P_a \times V_d$) (the pressure drop across the specimen times its dead volume) and also the quantity (Q_d/V_d) (the heat lost from the air across the specimen divided by its dead volume). The experimental results are to be compared to select the heat exchanger which is characterized by high heat transfer rate, low pressure losses and low dead volume.

All the experiments were carried out at different four values of coolant (water) mass flow rate to clarify the effect of the coolant *Reynolds* number. The results indicated no significant effect in the tested range (980 to 6200) of *Reynolds* number. The experimental results were discussed and plotted at the highest value of the coolant *Reynolds* number for each specimen.

The variation of the pressure drop ΔP_a versus the air mass flow rate for the specimens No. I, II, III, IV and V are shown in Fig. 8. It is clear that the pressure drop tends to increase with the increasing of air mass flow rate for the five specimens as it is expected. For the same values of the air mass flow rates, the specimen No. I has values of ΔP_a smaller than that of specimen No. II, because the dead volume of specimen No. I is greater than that of specimen No. II. Specimens No. III, IV and V have nearly the same

values of ΔP_a at the same values of the air mass flow rates, which lie between the values of ΔP_a of specimens No. I & II, although the dead volume of each of the specimens No. III, IV and V is less than that of specimen No. II. This is because the specimens No. III, IV and V have an elbow shape while the specimen No. II has a square section.

Figure 9 shows the variation of the heat transfer of specimens No. I, II, III, IV and V versus the air mass flow rate. It is clear that the specimen No. III has values of Q_a less than that of the others. Specimen No. III does not have the least number of tubes, but it is the only one which has a circular arrangement. Specimen No. II has the highest values of Q_a at the same value of the air mass flow rate. This is because specimen No. II has the highest number of the tubes.

As a first step of comparison; the quantities ($\Delta P_a \times V_d$) and (Q_a/V_d) are compared for the specimens no. I, II, III, IV and V versus the air flow rate.

Referring to Fig. 10, it is clear that the quantity ($\Delta P_a \times V_d$) tends to increase with the increase of air mass flow rate for the five specimens. The specimen no. III exhibits the lowest value of ($\Delta P_a \times V_d$). The reduction in ($\Delta P_a \times V_d$) is due to the small value of the dead volume of specimen No. III relative to the others and also the circular path of the air about the tubes which minimizes the disturbance resulted from eddies formation.

Referring to Fig. 11, the quantity (Q_a/V_d), is compared for the specimens no. I, II, III, IV and V versus the air flow rate. The specimen No. IV exhibits the highest value of (Q_a/V_d). The increase in the heat transfer rate is because the streamlines of air are not straight due to the circular path of air in an in-line arrangement of tubes which gives different angles of attack between the air and the tubes along the air path.

Referring to Fig. 12, the friction factor *f* is compared for the specimens no. I, II, III, IV and V versus *Reynolds* number. The specimen no. I exhibits the lowest values of the friction factor *f*. This is due to the minimum values of (ΔP_a) for the same values of air mass flow rates, consequently the same values of the mass flux.

Figure 13 shows Nu-Re plots that compares the specimens no. I, II, III, IV and V. The figure implies that the specimen no. I gives the highest *Nusselt* number compared to the other specimens at the same *Reynolds* number.

From the pervious discussion, it is evident that the circular arrangement of the tubes results in a considerable heat transfer rates as well as lower pressure loss and lower dead volume.

The three specimens no VI, VII and VIII in addition to specimen no III have the same circular path geometry and the tube bank arrangements. However, they have different values of tube pitches (S_n & S_p), hence different numbers of tubes and different values of dead volume.

Figure 14 shows the variation of the pressure drop ΔP_a versus air flow rate for specimens no. III, VI, VII and VIII. Referring to this figure, it is clear that the pressure drop ΔP_a tends to increase with the increase of air flow rate for the four specimens. Specimen No. III has values of ΔP_a higher than that of specimen No. VI at the same values of air mass flow rate. This is because the value of the pitch S_n of specimen No. VI is greater than that of specimen No. III. Specimens No. VI and VII have the same value of the pitch S_n, but specimen No. VII has higher values of ΔP_a compared to specimen No. VI. This is because the specimen No. VII has a value of the pitch S_p which is greater than that of specimen No. VI which increases the eddies between the tubes in the longitudinal direction. Specimen No. VIII has nearly the same number of tubes as specimen No. VII, but the former has lower values of ΔP_a compared to the latter. This is because the value of the pitch S_n of specimen No. VIII is greater than that of specimen No. VII and the value of the pitch S_p of specimen No. VIII is less than that of specimen No. VII.

Figure 15 shows the variation of the heat transfer (Q_a) of specimens No. III, VI, VII and VIII versus the air mass flow rate. It is clear that the specimen No. III has the lowest values of Q_a compared to the others although it has the highest number of tubes. This means that the heat transfer is increased by increasing the tube pitches within the investigated range.

As a second step of comparison; the quantities ($\Delta P_a \times V_d$) and (Q_a/V_d) are compared for the specimens no. III, VI, VII and VIII versus the air flow rate.

Figure 16 shows the variation of the quantity ($\Delta P_a \times V_d$) versus air flow rate for specimens no. III, VI, VII and VIII. Referring to this figure, it is clear that the quantity ($\Delta P_a \times V_d$) tends to increase with the increase of air flow rate for the four specimens. The figure shows that specimen No. III has the highest value of ($\Delta P_a \times V_d$) while specimen No. VIII has the lowest one.

Figure 17 shows that the specimens No. VI, VII and VIII have nearly the same values of (Q_a/V_d), which are slightly greater than that of specimen No. III. This means that the number of tubes does not have a significant effect on the quantity (Q_a/V_d).

Referring to Fig. 18, it is noted that the specimen no. III has the lowest friction factor *f* when compared with the

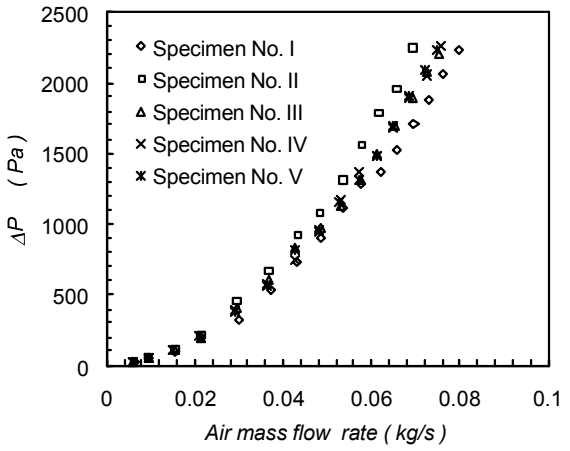

Fig. 8: Variation of the pressure drop versus air mass flow rate

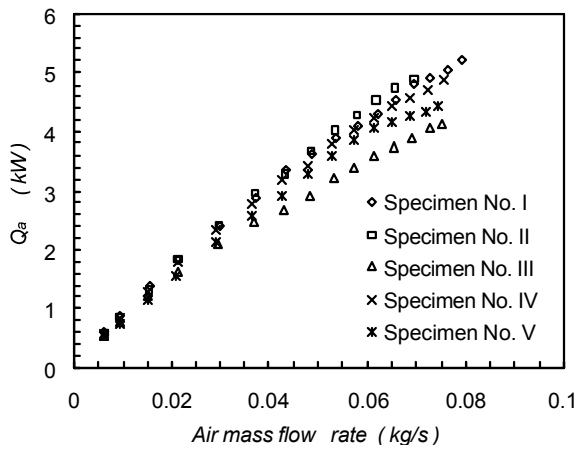

Fig. 9: Variation of the heat transfer versus air mass flow rate

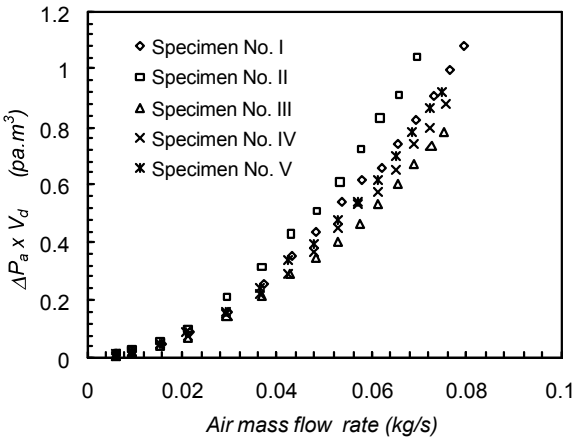

Fig. 10: Variation of the quantity (? P_a x V_d) versus air mass flow rate

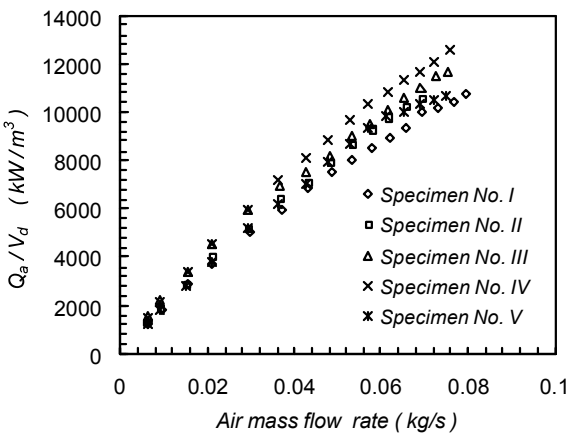

Fig. 11: Variation of the quantity (Q_a / V_d) versus air mass flow rate

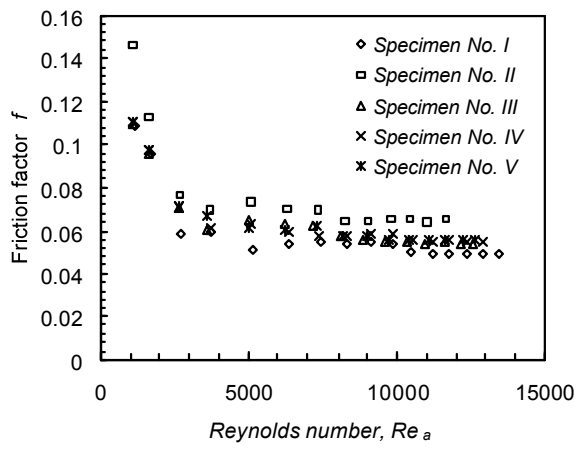

Fig. 12: Variation of the friction factor versus Reynolds number

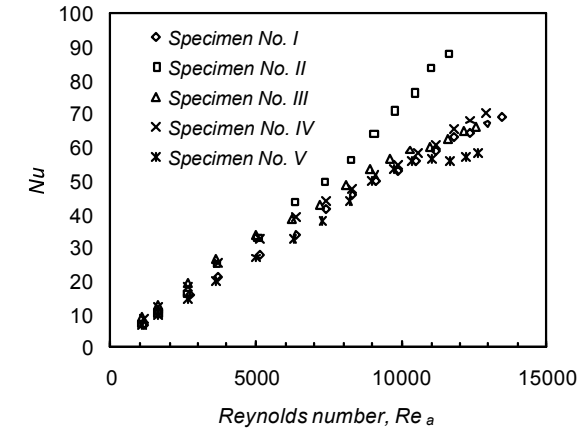

Fig. 13: Variation of Nusselt number versus Reynolds number

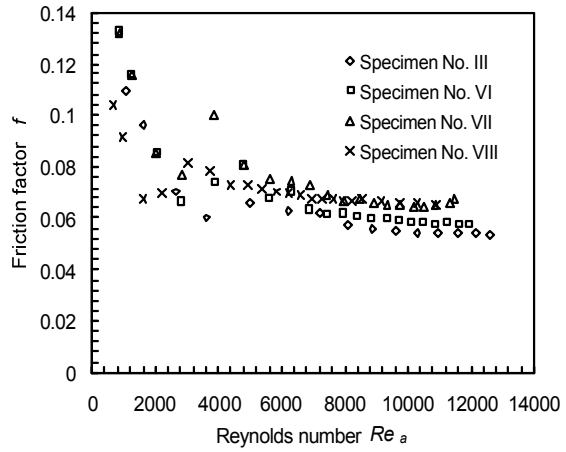

Fig. 14: Variation of the pressure drop ? P_a versus air mass flow rate

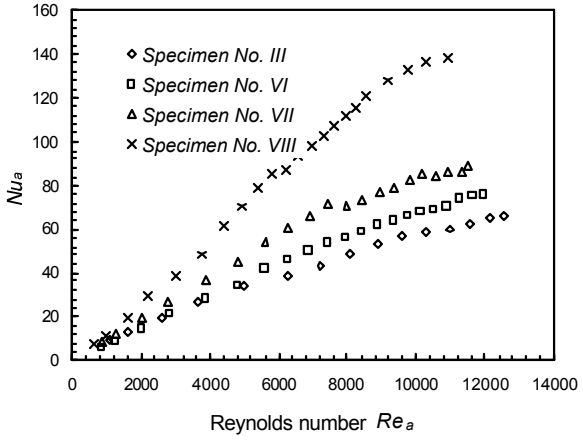

Fig. 15: Variation of the heat transfer Q_a versus air mass flow rate

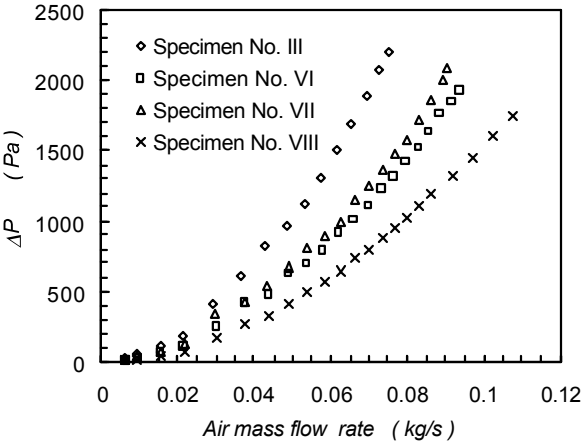

Fig. 16: Variation of the quantity (? P_a x V_d) versus air mass flow rate

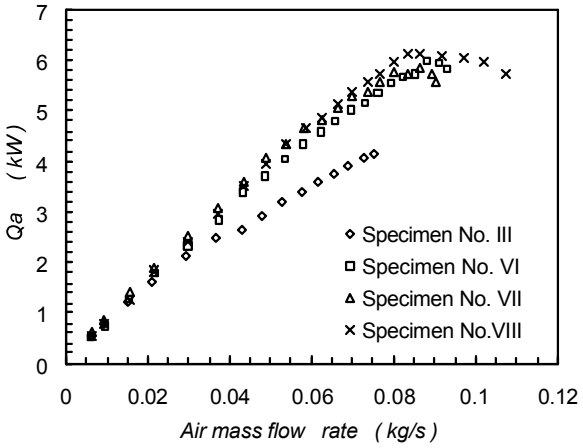

Fig. 17: Variation of the quantity (Q_a / V_d) versus air mass flow rate

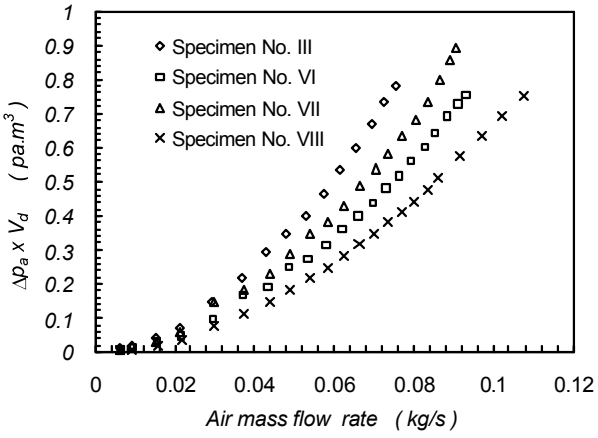

Fig. 18:Variation of the friction factor versus Reynolds number

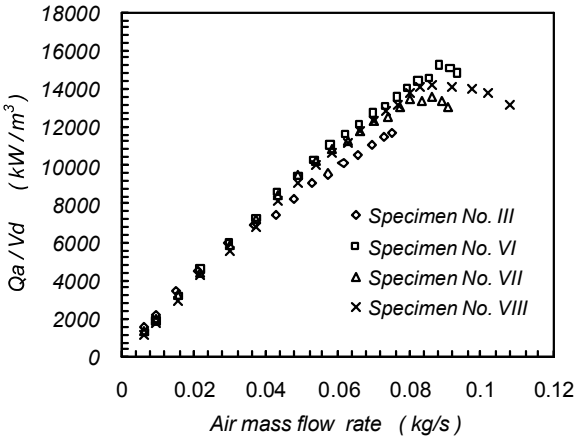

Fig. 19: Variation of Nusselt number versus Reynolds number

Table 1:

Specimen No.	Range	C_1	C_2	C_3
I	1100 = Re_a < 2700	0	-3.174×10^{-5}	0.1453
	2700 = Re_a < 10500	6.476×10^{-11}	-1.646×10^{-6}	0.06239
	10500 = Re_a < 10500	0	-2.110×10^{-7}	0.05189
II	1100 = Re_a < 2700	0	-4.313×10^{-5}	0.1892
	2700 = Re_a < 8200	-1.480×10^{-10}	9.567×10^{-8}	0.07543
	8200 = Re_a < 11700	0	1.746×10^{-8}	0.06486
III	1090 = Re_a < 2600	0	-2.517×10^{-5}	0.1364
	2600 = Re_a < 8900	-1.379×10^{-10}	1.297×10^{-7}	0.06832
	8900 = Re_a < 12600	0	-3.680×10^{-7}	0.05856
IV	1100 = Re_a < 2700	0	-2.474×10^{-5}	0.1376
	2700 = Re_a < 10600	2.387×10^{-10}	-4.601×10^{-6}	0.07916
	10600 = Re_a < 12900	0	-6.525×10^{-8}	0.05590
V	1100 = Re_a < 2600	0	-2.525×10^{-5}	0.1377
	2600 = Re_a < 9700	1.881×10^{-10}	-4.238×10^{-6}	0.08029
	9700 = Re_a < 12600	0	-3.207×10^{-8}	0.05596
VI	800 = Re_a < 2800	0	-3.375×10^{-5}	0.1580
	2800 = Re_a < 9700	-3.795×10^{-10}	2.546×10^{-6}	0.06765
	9700 = Re_a < 11900	0	-2.348×10^{-7}	0.06107
VII	800 = Re_a < 2800	0	-2.875×10^{-5}	0.1552
	2800 = Re_a < 8000	-1.018×10^{-9}	7.084×10^{-6}	0.07237
	8000 = Re_a < 11500	0	-3.628×10^{-7}	0.06937
VIII	600 = Re_a < 2200	0	-3.872×10^{-5}	0.1289
	2200 = Re_a < 7900	-6.458×10^{-10}	5.183×10^{-6}	0.06403
	8000 = Re_a < 10900	0	-5.862×10^{-7}	0.07171

Table 2:

Specimen No.	Range	A	B
I	1100 = Re_a < 13500	9.327×10^{-3}	0.9389
II	1100 = Re_a < 11700	3.691×10^{-3}	1.072
III	1100 = Re_a < 12600	3.598×10^{-2}	0.7995
IV	1100 = Re_a < 12900	2.203×10^{-2}	0.8520
V	1100 = Re_a < 12600	1.149×10^{-2}	0.9112
VI	800 = Re_a < 11900	1.116×10^{-2}	0.9478
VII	800 = Re_a < 11500	1.776×10^{-2}	0.9202
VIII	600 = Re_a < 10900	7.502×10^{-3}	1.069

specimens no. VI, VII and VIII at the same *Reynolds* number Re_a. It is also noted that the specimens No. VII and VIII have nearly the same friction factor for the values of *Reynolds* number higher than 8000.

Referring to Fig. 19, the specimen no. VIII has the highest *Nusselt* number compared to the other specimens at the same *Reynolds* number. It shows adequate accordance with the diagram of the heat transfer.

The heat exchanger effectiveness (ε) was calculated from equation (9) in which the heat transfer rate Q_{ave} was calculated as the average of the air and water side values.

Referring to Fig. 20, the effectiveness (ε) was plotted versus the number of transfer units (*NTU*) calculated from equation (10). This was done using the experimental results of all the heat exchangers which were tested in the present work. The relation was correlated as follows:

$$\varepsilon = 0.6602\times NTU^{0.7527}$$

which is shown as the solid line in Fig. 20. The dotted line will be discussed in the section of "Comparison with previous work" as shown below.

Referring to Fig. 12 and 18 for friction factor and Fig. 13 and 19 for *Nusselt* number, a number of correlations were deduced for each specimen. The friction factor correlation has the following form, $f = C_1\times Re_a^2 + C_2\times Re_a + C_3$, while the *Nusselt* Number correlation has the following form, $\bar{Nu} = A\times Re_a^B$. The constants C_1, C_2 and C_3 are shown in Table 1 and the constants A and B are shown in Table 2. These correlations can be used in the calculations of heat transfer and pressure losses in Stirling machines.

COMPARISON WITH PREVIOUS WORK

It is very hard to make a complete comparison between the experimental data of the heat exchangers

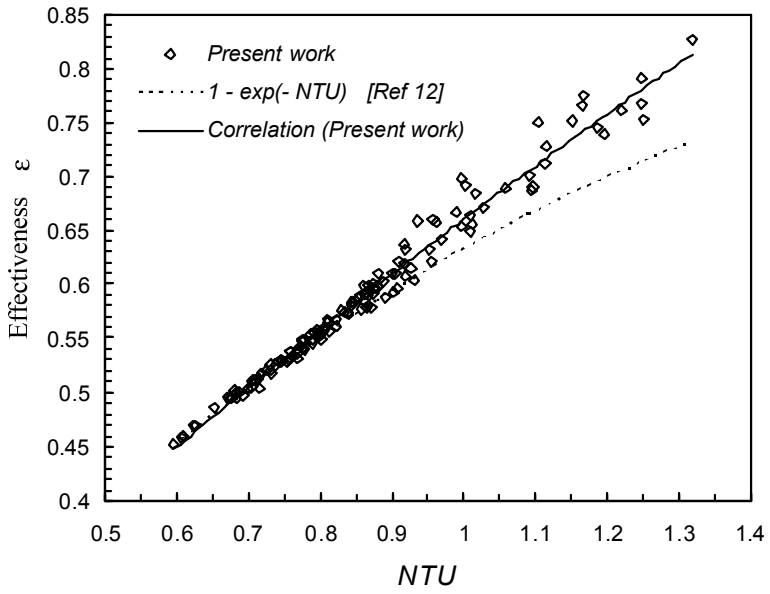

Fig. 20: Comparison between the present work and other heat exchangers for (e & NTU)

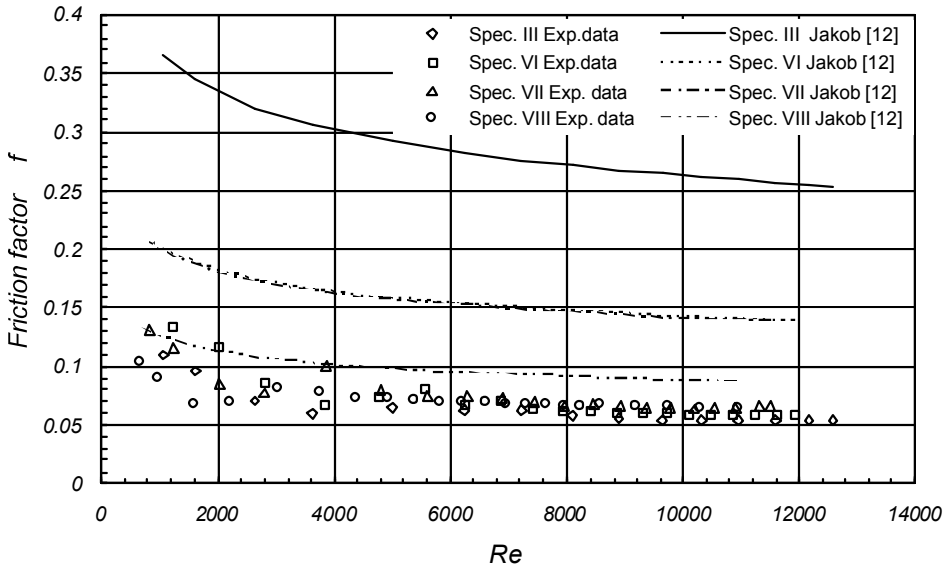

Fig. 21: Comparison between the present work and Jakob for (*f & Re*)

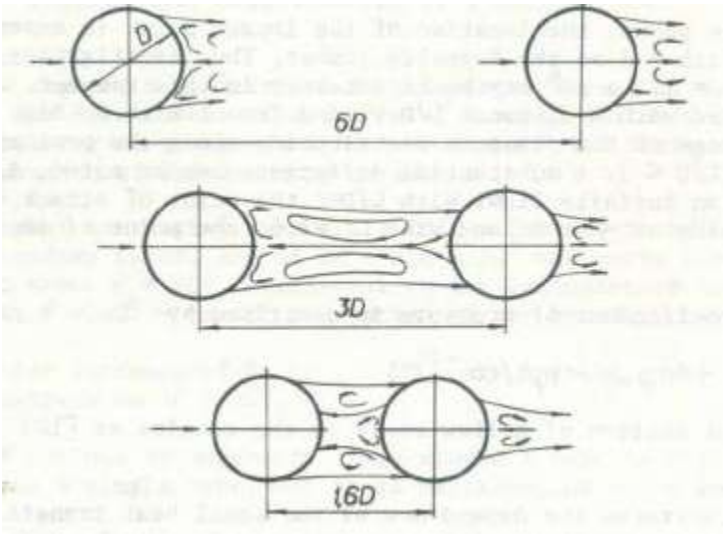

Fig. 22: Pattern of flow past a tube in a longitudinal row [13]

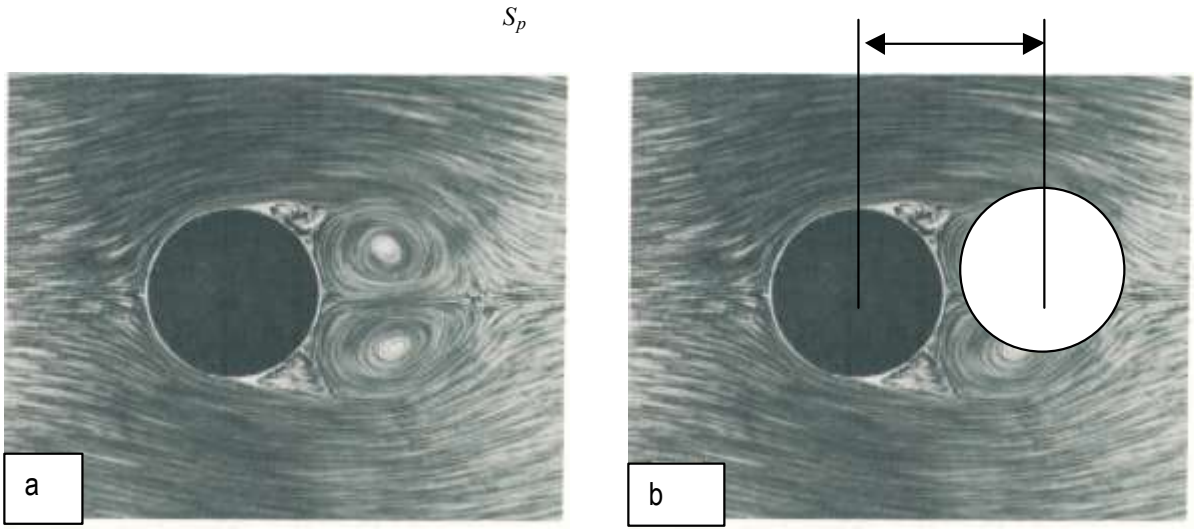

Fig. 23

(a) Picture of the pattern of the flow past a tube [14].

(b) The location of the Second tube in the present work (white circle).

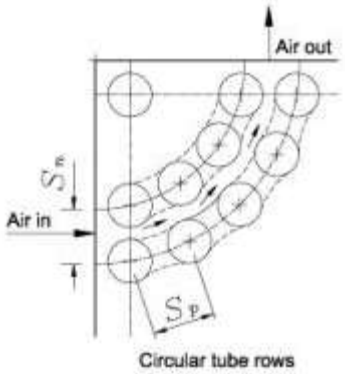

Fig. 24: Expected imaginary corrugated sheet of the tubes in the present work

which are suggested in this work and the other heat exchangers. This is because of the difference of the direction of flow outside the tubes between the heat exchangers suggested in the present work and the others. So, the comparison given below can be used only as a guide.

Figure 20 shows a comparison between the values of the effectiveness (ε) found from the experimental results of all the heat exchangers used in the present work and the values of the effectiveness (ε) calculated from the relation ($\varepsilon = 1\text{-}e^{-NTU}$) given by Holman [12] assuming that $C^* \approx 0$ for all the heat exchangers. It can be seen that the experimental results are too close to that of the previous work for NTU=0.75. For higher values of NTU, the experimental results give higher values of effectiveness.

Figure 21 shows the comparison between the empirical relation of the friction factor *f* which is given by Holman [12] for in-line arrangements and the values of the friction factor *f* of the specimens no. III, VI, VII, VIII, assuming in-line arrangement with circular path for them. It is clear that the empirical relations [12] have values higher than the present data, but have the same trend.

The investigations of Holman[12] relation, indicates that the friction factor *f* increases as the pitch S_p or/and S_n decreases.

For in-line banks, the location of the impact point is dependent on the longitudinal pitch S_p and on the *Reynolds* number. With $S_p/d=6$ the point of attack and the point of impact coincide at φ=0, while with $S_p/d=1.6$, the point of impact is shifted to φ=75°, as shown in Fig. 22 [13].

The effect of turbulence on a typical flow pattern across a tube is indicated by the picture presented in Fig. 23a taken from Fraas [14]. A stagnant region then begins to develop in the wake of the tube and eddies form and grow, distorting the flow pattern. Referring to this picture, it is clear that the eddies extend to a distance nearly equal to the tube diameter. According to Fig. 22c, it can be concluded that if the second tube is located at a distance $S_p<1.6\ d$ as shown in Fig. 23b, the major portion of the eddies will be eliminated and the point of impact is shifted to φ 90. There are no eddies on the rear surface of the first tube and no impact force on the front surface of the second tube. The same can be said about any two consecutive tubes. Then the intermediate surfaces of the tubes have no effect. The surfaces of the tubes in the longitudinal row are expected to be as a corrugated sheet as shown in Fig. 24. As a result, the pressure drop will be decreased to a small value. This is the case of the present work where the value of S_p/d ranges between 1.20 and 1.34. This explains why the friction factor in the present work is less than that calculated from the relation given by Holman [12].

CONCLUSIONS

Empirical correlations were deduced to describe the results extensively. The following conclusions were found for the air-side heat transfer and pressure drop characteristics of elbow-bend geometry and tube bank arrangements within the range studied in this work.

1. The circular elbow-bend geometry with circular tube bank arrangement is the best heat exchanger compared to the other arrangements studied in the present work.
2. The number of tubes arranged in a certain space does not have the main effect on the pressure drop and the heat exchange rate if the tube pitch S_n is less than 1.425 and S_p is less than 1.34 (the investigated range).
3. The tube bank arrangement has a main effect on the pressure drop in the heat exchanger.
4. For the circular elbow bend geometry, if the tubes are arranged in a circular path, the pressure drop increases as the transverse pitch S_n decreases and the longitudinal pitch S_p increases.
5. Increasing any or both of the longitudinal or transverse pitches slightly increases the rate of the heat exchange. However, the relation between them is not clear.

REFERENCES

1. Wamoto, S., F. Toda, K. Hirata, M. Takeuchi and T.Yamamoto, 1997. Comparison of Low-and High Temper-ature Differential Stirling Engines, 8th ISEC, 97004, Ancona, Italy.
2. Hoshino, T., T. Fujihara, S. Ogiwara and K. Eguchi, 1997. Performance Evaluations of Space-based Stirling Engine-NALSEM 500, 8th ISEC, 97018, Ancona, Italy.
3. Chang, W.S., D.K. Shin and S.Y. Kim, 1997. Study on the Low Cost Stirling Engine and its Performance Test Results. 8th ISEC, 97056, Ancona, Italy.
4. Liu, Biao and Li Xianrui, 1997. Design of A Domestic Stirling-Electric Power system, 8th ISEC, 97060, Ancona, Italy.
5. Kongtragool, B. and S. Wongwises, 2006. A Thermodynamic Analysis of a Stirling Engine Including Dead Volumes of Hot Space, Cold Space and Regenerator", Renewable Energy, 31: 345-359.

6. El-Ehawany, A.A., M.M. Kamel, G.M. Hennes and E.I. Eid, 1999. An Experimental Investigation of Block Type Heat Exchangers. Helwan University, Faculty of Enging, Mataria, Cairo, August. Enging. Res. J., 64: 83-99.
7. Wang, C., Y. Lin and C. Lee, 2000. An Air Side Correlation for Plain Fin-and-Tube Heat Exchangers in Wet Conditions. Intl. J. Heat Mass Transfer, 43: 1869-1872.
8. Yan, W. and P. Sheen, 2000. Heat Transfer and Friction Characteristics of Fin-and-Tube Heat Exchangers. Intl. J. Heat Mass Transfer, 43: 1651-1659.
9. Kim, N.H., B. Youn and R.L. Webb, 1999. Air-Side Heat Transfer and Friction Correlations for Plain Fin-and-Tube Heat Exchangers With Staggered Tube Arrangements. Transactions of the ASME 662/ 121: 662-667, August.
10. BSI, 1981. Methods of Measurement of Fluid Flow in Closed Conduits. Part 1, British Standards Institution, BS 1402: Section 1.1.
11. Holman, J.P., 2001. Experimental Methods for Engineers. International Edition, Seventh Edition, McGraw-Hill New York, USA.
12. Holman, J.P., 2002. Heat Transfer, Ninth Edition, New York, McGraw-Hill Inc.
13. Kakac, S., A.E. Bergles and F. Mayinger, 1981. Heat Exchanger Thermal-Hydraulic Fundamentals and Design. Hemisphere Publishing Corporation.
14. Fraas, A.P. and M.N. Ozisik, 1965. Heat Exchanger Design. John Wiley and Sons Inc.

Nomenclature

A	area	m^2
B	heat exchanger width	m
C	heat capacity rate	W/ K
C_P	specific heat at constant pressure	$J/kg\ .\ K$
d	tube diameter	m
f	friction factor	----
G	mass flux of the air based on the minimum flow area	$kg/m^2.s$
h	heat transfer coefficient	$W/m^2.K$
k	thermal conductivity	$W/m\ .K$
L	effective length of tube	m
	mass flow rate	kg/s
n	number of water passes	-----
N	number of tube rows	-----
N_{total}	total number of tubes	-----
Nu	*Nusselt* number	-----
NTU	number of transfer units	-----
$?P$	pressure drop	Pa
	heat transfer rate	W
Re	*Reynolds* number	-----
S	tube spacing (pitch)	m
S_v	surface area of heat transfer to volume ratio	m^2/m^3
T	temperature	K
U	overall heat transfer coefficient	$W/m^2.K$
V_{total}	total volume of the specimen	m^3
V_d	dead volume	m^3
	dynamic viscosity	$Pa.s$
	density	$/\ m^3$
ø	porosity	-----
ε	heat exchanger effectiveness	-----
φ	impact angle of the stream lines	rad

Subscripts

a	air side	n	transverse
ave	average value	o	outer
i	inner	p	longitudinal
max	maximum value	s	tube surface
min	minimum value	w	water side